

# We are IntechOpen, the world's leading publisher of Open Access books Built by scientists, for scientists

6,900

Open access books available

186,000

International authors and editors

200M

Downloads

Our authors are among the

154

Countries delivered to

TOP 1%

most cited scientists

12.2%

Contributors from top 500 universities



WEB OF SCIENCE™

Selection of our books indexed in the Book Citation Index  
in Web of Science™ Core Collection (BKCI)

Interested in publishing with us?  
Contact [book.department@intechopen.com](mailto:book.department@intechopen.com)

Numbers displayed above are based on latest data collected.  
For more information visit [www.intechopen.com](http://www.intechopen.com)



---

# Computer-Aided Determination of the Air-Side Heat Transfer Coefficient and Thermal Contact Resistance for a Fin-and-Tube Heat Exchanger

---

Jan Taler, Paweł Ochoń, Dawid Taler and  
Marzena Nowak-Ochoń

Additional information is available at the end of the chapter

<http://dx.doi.org/10.5772/60647>

---

## 1. Introduction

Plate fin-and-tube heat exchangers with oval tubes attract the broad scientific interest due to its large thermal efficiency, significant heat transfer rate between the mediums and compact shape [1-10]. The heat exchangers of this type are widely used in industrial plants and installations, as air-coolers, convectors for home heating and waste heat recovery for gas turbines. The large thermal efficiency is achieved by using the external fins, fixed at the oval tubes of the heat exchanger [1-3]. Mostly, fin-and-tube heat exchangers operate in the cross-flow arrangements. A liquid (water or oil) flows through the tubular space of the heat exchanger, and gas (air, flue gas) flows across the intertubular space of the heat exchanger. Due to the use of external fins, a heat transfer rate increases when compared with tubes without fins. Moreover, the application of the oval tube shape reduces the pressure drop and improves heat transfer conditions on the gas side when compared to the circular shape [4-14, 17]. Since plate fin-and-tube heat exchangers operate in a cross-flow arrangement with the complex path of gas flow, hence in order to determine the velocity field and heat transfer characteristics, the numerical methods must be used [15-16, 18-25]. For the gas flow, with the use of the commercial CFD codes (ANSYS CFX [31], FLUENT), it is possible to calculate the local values of heat transfer coefficient. However, it is impossible to incorporate these values into the analytical formulas, which allow determining the overall heat transfer coefficient. These formulas are fundamental when designing cross-flow heat exchangers and use the average not local values of heat transfer coefficient. Therefore in this study authors present different methods for determination of the average heat transfer coefficient for gas flow in a plate fin-and-tube heat exchanger using the CFD simulations. The values of the heat transfer coefficient obtained using

the heat transfer formulas for the Nusselt number, determined with the CFD simulations, can be directly implemented in the thermal designing procedure of the cross-flow heat exchangers. The results of the numerical computations will be validated experimentally, using the procedures described in [14, 17, 20].

The numerical studies of the performance of plate fin-and-tube heat exchangers encounter difficulties in the proper prediction of the total gas side temperature difference. This problem occurs, because of the flow maldistribution of mediums flowing through the heat exchanger and thermal contact resistance between the fin and tube. The thermal contact resistance, which can significantly reduce the thermal performance of heat exchange apparatus, is difficult to determine [15, 19]. It is considerable when the oval tubes are inserted into the holes, which are stamped in metal strips. Then, the tubes are expanded to create the so-called interference fit. Since the gap exists between the fin and tube, the corrosion residuals can cumulate within the gap, leading to the decrease in heat transfer ability. It should be noted, that the direct investigation of thermal contact resistance is difficult to conduct. Therefore, the alternative methods are needed. This study discusses the alternative approach to determining the thermal contact resistance between fin and tube, based on the CFD simulation and experimental data. Moreover, the methods for determining the heat transfer coefficient correlations for the air side are also presented.

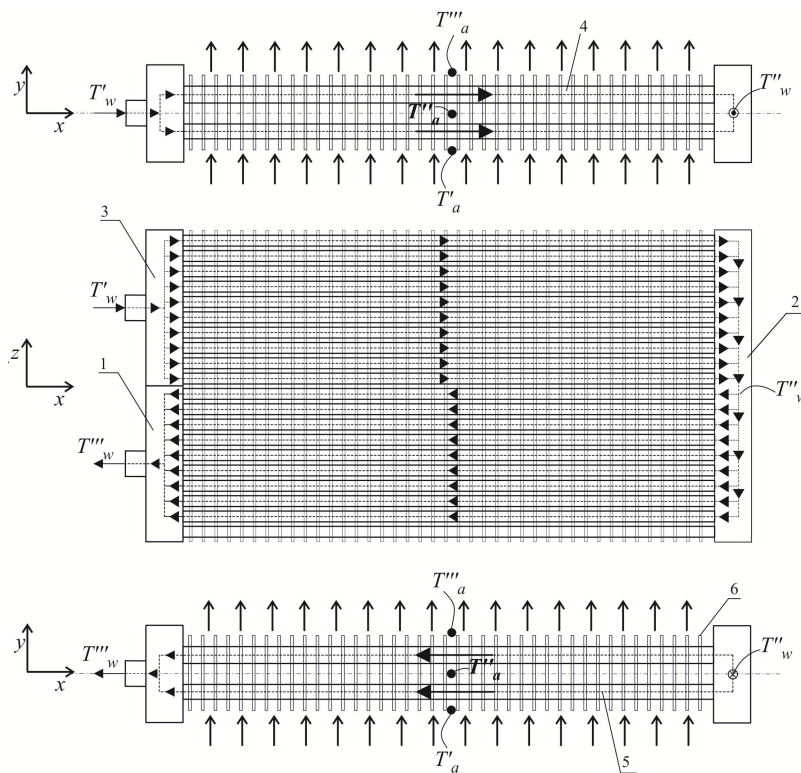
## 2. Test facility – fin-and-tube heat exchanger with oval tubes

Figure 1 presents the scheme of a car radiator, for which the heat transfer coefficients will be determined [19].

The heat exchanger is used for cooling the spark ignition engine with a cubic capacity equal to 1, 580 cm<sup>3</sup>. Hot water, which flows inside the aluminum tubes of the heat exchanger, is cooled down by the air flowing across the intertubular space.

The two-pass /two-row fin and tube heat exchanger is considered. The following characteristics are given:

- Total number of tubes: 38, including 20 tubes in the first pass and 18 tubes in the second
- The tube length is  $L_t = 0.52$  m.
- The radiator width, height, and thickness is equal to 520 mm, 359 mm and 34 mm, respectively
- The aluminum ( $k = 207$  W/(m K)) oval tubes of outer diameters  $d_{min} = 6.35$  mm and  $d_{max} = 11.82$  mm, respectively, with thickness of  $\delta_t = 0.4$  mm are used
- Total number of plate fins (359 mm height, 34 mm width and 0.08 mm thickness) along the tube length is 520
- The fin pitches in the perpendicular and longitudinal directions to the air flow are as follows:  $p_1=18.5$  mm  $p_2=17$  mm (Fig. 2, [19])



**Figure 1.** Flow scheme of two-row car radiator with two passes: 1 – inlet manifold, 2 – intermediate manifold, 3 – outlet manifold, 4 – second row of oval tubes, 5 – first row of oval tubes, 6 – plate fin.

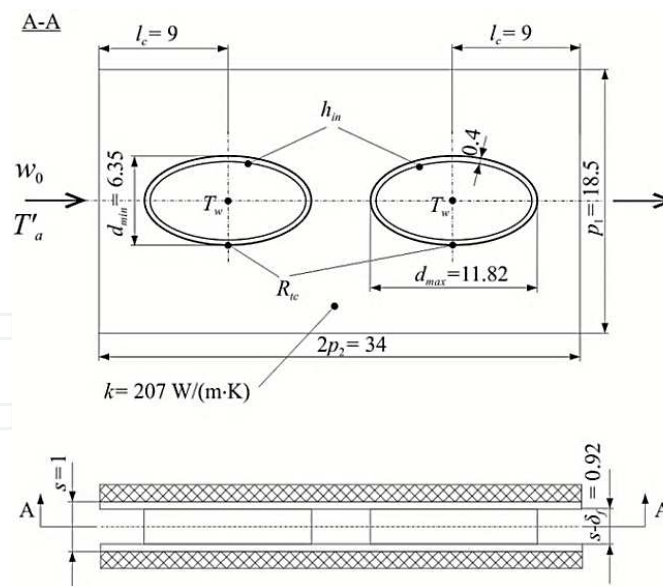


**Figure 2.** Scheme of the narrow air flow passage across the car radiator.

The path of the water flow is U-shaped, this means that the water reverses in the intermediate manifold. In the first pass (upper), the hot water with temperature  $T'_w$  flows from the inlet header (1) through the two rows of the oval tubes, with the length  $L_t = 0.52$  m. Then, in the

intermediate header (2), the mixing of the water streams from the first (4) and second (5) row occurs. The intermediate temperature of the water is equal to  $T''_w$ . Next, the water reverses and flows into the two rows of the tubes located in the second (lower) pass. Finally, the liquid, cooled down to temperature  $T'''_w$  flows out of the heat exchanger through the outlet manifold (3). The air with inlet temperature  $T'_a$  flows in the normal direction to the both rows of the finned tubes. After the first and second row, air temperature is  $T''_a$  and  $T'''_a$ , respectively (Fig. 1). The plate fins (6) are used to enhance the heat transfer from the air side.

For the CFD calculations presented in this paper (section 4), the flow in a narrow passage formed between two consecutive fins is considered.

### 3. Experimental methods of determining the air-side heat transfer coefficient in fin-and-tube heat exchanger

The experimental-numerical method for determining the average air-side heat transfer coefficient was described in details in ref. [14, 17]. Moreover, in ref. [17], the detailed list of measurement points, used in this work, is presented. The experimental-numerical method involves the performance tests of a car radiator (Fig. 1) and allows to obtain the formulas for the Nusselt number for the air and water flows. During the measurements the inlet and outlet air temperatures ( $T'_a$  and  $T'''_a$ ), the inlet and outlet water temperatures ( $T'_w$  and  $T'''_w$ ), the volumetric mass flow rate of water  $\dot{V}_w$ , and the inlet velocity of the air  $w_0$ , are determined. The following change ranges of  $T'_a$ ,  $T'''_a$ ,  $\dot{V}_w$ ,  $T'_w$ ,  $T'''_w$  and  $w_0$  were examined:

- $T'_a = 12.5 \text{ }^\circ\text{C} - 15 \text{ }^\circ\text{C}$ ,
- $T'''_a = 38.51 \text{ }^\circ\text{C} - 57.66 \text{ }^\circ\text{C}$ ,
- $\dot{V}_w = 865.8 \text{ dm}^3/\text{h} - 2186.40 \text{ dm}^3/\text{h}$ ,
- $T'_w = 61.0 \text{ }^\circ\text{C} - 71.08 \text{ }^\circ\text{C}$ ,
- $T'''_w = 49.58 \text{ }^\circ\text{C} - 63.83 \text{ }^\circ\text{C}$ ,
- $w_0 = 1 \text{ m/s} - 2.2 \text{ m/s}$ .

The value of the experimental heat transfer coefficient  $h_{a,i}^e$  for the air flow is determined based on the condition that the calculated outlet temperature  $T_{w,i}'''(h_{a,i}^e)$  of water must be equal to the measured temperature  $(T_{w,i}''')^e$ , where  $i=1, \dots, n$  is the dataset number. The following non-linear algebraic equation must be solved for each dataset to determine  $h_{a,i}^e$ :

$$(T_{w,i}''')^e - T_{w,i}'''(h_{a,i}^e) = 0, i = 1, \dots, n \quad (1)$$

where  $n$  is the number of datasets. This study employs the mathematical model of the heat exchanger developed in [11] to calculate the water outlet temperature  $T_{w,i}'''$  as a function of the

heat transfer coefficient  $h_{a,i}^e$ . The heat transfer coefficient for the air flow  $h_{a,i}^e$  is determined by searching for such a preset interval that makes the measured outlet temperature of water  $(T_{w,i}^m)^e$  and the computed outlet temperature  $T_{w,i}^m$  the same. The outlet water temperature  $T_{w,i}^m(h_{a,i}^e)$  is calculated at each search step. Next, a specific form is adopted for the formula on the air-side Colburn factor  $j_a = j_a(\text{Re}_a)$ , with  $m = 2$  unknown coefficients. The least squares method allows to determine the coefficients  $x_1, x_2$  under the condition:

$$S_{\min} = \sum_{i=1}^n \left[ j_{a,i}^e - j_{a,i}(x_1, x_2) \right]^2 = \min, m \leq n \quad (2)$$

where:

$$j_a = \text{Nu}_a / (\text{Re}_a \text{Pr}_a^{1/3}) \quad (3)$$

is the air Colburn factor and  $\text{Pr}_a = \mu_a c_{pa} / k_a$  is the air Prandtl number. The  $\text{Nu}_a = h_a d_h / k_a$  and  $\text{Re}_a = w_{\max} d_h / \nu_a$  are the air Nusselt and Reynolds numbers, respectively. The velocity  $w_{\max}$  is the air velocity in the narrowest free flow cross-section  $A_{\min}$ . The symbol  $j_{a,i}^e$  is the experimentally determined Colburn factor, and  $j_{a,i}$  is the  $j$ -factor calculated with the approximating function for the set value of the Reynolds number  $\text{Re}_{a,i}$ . The Colburn factor  $j_a$  is approximated by a power-law function:

$$j_a = x_1 \text{Re}_a^{x_2} \quad (4)$$

The unknown coefficients  $x_1$  and  $x_2$  are determined by the Levenberg-Marquardt method [35], using the Table-Curve program [36]. Combining Equations (3) and (4) one gets:

$$\text{Nu}_a = x_1 \text{Re}_a^{(1+x_2)} \text{Pr}_a^{1/3} \quad (5)$$

The  $w_{\max}$  air velocity in the narrowest cross-section of flow  $A_{\min}$  is defined as:

$$w_{\max} = \frac{sp_1}{A_{\min}} \left( \frac{\bar{T}_a + 273.15}{T'_a + 273.15} \right) w_0 \quad (6)$$

where  $A_{\min}$  is

$$A_{\min} = (s - \delta_f)(p_1 - d_{\min}) \quad (7)$$

The equivalent diameter for the air flow passage  $d_h$  is [17, 18-19]:

$$d_h = \frac{4A_{min}L_t}{A_f + A_e}, \quad (8)$$

where the fin surface of a single passage  $A_f$  is:

$$A_f = 2 \cdot 2(p_1 p_2 - A_{oval}) = (4p_1 p_2 - \pi d_{min} d_{max}), \quad (9)$$

the tube external surface between two fins  $A_e$  is:

$$A_e = 2 \cdot P_o (s - \delta_f). \quad (10)$$

For the given parameters of the air-flow passage, the equivalent hydraulic diameter is  $d_h = 0.00141$  m. The arithmetic average air temperature  $\bar{T}_a$  taken from the inlet air temperature  $T_a'$  and the outlet air temperature  $T_a''$  is used to evaluate the thermal properties.

Air-side heat transfer correlations found in this chapter will be compared with the correlations of Kröger [37, 38].

The air-flow Nusselt number correlations, determined via the measurements, are listed in Table 1 [19, 20]. These correlations are paired with the water-flow heat transfer formulas, given in the literature [39- 41]. The correlations presented in Table 1 were employed to determine the outlet temperature of water  $T_{w,i}''$  using the heat exchanger model [11].

The water flow criteria numbers are:  $Nu_w = h_{in} d_t / k_w$  and  $Re_w = w_w d_t / \nu_w$ . The friction factor  $\xi$  is defined as:

$$\xi = \frac{1}{(1.82 \log Re_w - 1.64)^2} = \frac{1}{(0.79 \ln Re_w - 1.64)^2} \quad (11)$$

The mean water velocity in a single tube –  $w_w$  is calculated using the total volumetric flow rate  $\dot{V}_w$  as follows:

$$w_w = \dot{V}_w / (n_{tp} A_{w,in}), \quad (12)$$

where  $n_{tp}$  is the number of tubes in a single pass of the heat exchanger and  $A_{w,in}$  is the cross-sectional area of the flow related to one tube.

No.	Correlation - experiment	Estimated parameters
1	$Nu_a = x_1 Re_a^{x_2} Pr_a^{1/3} \text{ (experiment)}$ $Nu_w = \frac{(\xi/8)(Re_w - 1000)Pr_w}{1 + 12.7\sqrt{(\xi/8)(Pr_w^{2/3} - 1)}} \left[ 1 + \left( \frac{d_t}{L_t} \right)^{2/3} \right]$ [39]	$S_{min} = 0.6678 \text{ K}^2$ $s_t = 0.1102 \text{ K}$ $x_1 = 0.1117 \pm 0.0024,$ $x_2 = 0.6469 \pm 0.0045$
2	$Nu_a = x_1 Re_a^{x_2} Pr_a^{1/3} \text{ (experiment)}$ $Nu_w = \frac{(\xi/8)(Re_w - 1000)Pr_w}{k_1 + 12.7\sqrt{(\xi/8)(Pr_w^{2/3} - 1)}} \left[ 1 + \left( \frac{d_t}{L_t} \right)^{2/3} \right]$ $k_1 = 1.07 + \frac{900}{Re_w} + \frac{0.63}{(1 + 10Pr_w)}$ [40]	$S_{min} = 1.2799 \text{ K}^2$ $s_t = 0.1540 \text{ K}$ $x_1 = 0.1309 \pm 0.00418,$ $x_2 = 0.6107 \pm 0.0559$
3	$Nu_a = x_1 Re_a^{x_2} Pr_a^{1/3} \text{ (experiment)}$ $Nu_w = \frac{(\xi/8)Re_w Pr_w}{1 + 8.7\sqrt{(\xi/8)(Pr_w - 1)}} \left[ 1 + \left( \frac{d_t}{L_t} \right)^{2/3} \right]$ [41]	$S_{min} = 1.4034 \text{ K}^2$ $s_t = 0.1569 \text{ K}$ $x_1 = 0.1212 \pm 0.0398,$ $x_2 = 0.6258 \pm 0.0595$
4	$Nu_a = x_1 Re_a^{x_2} Pr_a^{1/3} \text{ (experiment)}$ $Nu_w = \frac{\xi/8(Re_w - x_3)Pr_w}{1 + x_4(\xi/8)^{1/2}(Pr_w^{2/3} - 1)} \left[ 1 + \left( \frac{d_t}{L_t} \right)^{2/3} \right]$ [19]	$S_{min} = 1.2117 \text{ K}^2$ $s_t = 0.1496 \text{ K}$ $x_1 = 0.1012, x_2 = 0.6704$ $x_3 = 1404.4860, x_4 = 11.9166$

**Table 1.** Nusselt number formulas for the air flow  $Nu_a$  obtained from the measurements

The water-flow equivalent hydraulic diameter  $d_t$  is calculated as

$$d_t = \frac{4A_{w,in}}{P_{in}}, \tag{13}$$

where  $P_i$  denotes the oval perimeter (referred to inner tube wall). In this study, the water side hydraulic diameter  $d_t$  is 0.00706 m.

#### 4. Determining of the air-side heat transfer coefficient using CFD simulations

The CFD simulations [32] were performed to model the heat and fluid flow processes in the air-flow passage, shown in Fig. 2. As a result, the air temperature and velocity are determined. Moreover, with the application of a conjugate heat transfer treatment, the wall temperature of fin and tube are calculated. A similar modeling approach for the gas flow in fin-and-tube heat exchangers was used in papers [15, 18-20]. The approach allows to simplify the computational

domain and reduce the computational costs. In this study, the CFD software ANSYS CFX - release 13.0 [31] was used. The phenomenon of air flow across the passage is complex e.g. flow is turbulent at the heat exchanger inlet and laminar between the fins. Hence, the SST turbulence model with Gamma-theta transitional turbulence formulation [33, 34] is used in computations. The model allows to study at the same time both the laminar and turbulent flows.

The element based finite volume method is used to discretize the differential governing equations. The coupled solver is used for the momentum and continuity equations. The Rhie-Chow interpolation scheme with the co-located grid is applied for pressure. The so-called “high resolution” scheme is used to discretize the convective terms [31].

Fig. 3 shows the discrete model and the applied boundary conditions. The model consists of three heat transfer domains: air (1), fin (2), and tube (3). The inlet boundary condition, where the values of air velocity  $w_0$  and temperature  $T'_a$  are prescribed, is denoted as (I). At the outlet boundary (II) the pressure level was held constant at 1 bar. At the inner tube surface (III) the convective boundary condition is applied to model the heat transfer from the water to the tube wall. The water-side heat transfer coefficient  $h_{in}$  was determined from the experimental correlation for  $Nu_w$  given in Table 1. The bulk temperature of the water  $\bar{T}_w$  flowing through the tube is calculated as the arithmetic average of the measured temperatures:  $T'_w$  and  $T'''_w$ .

The thermal resistance between external tube surface and fin  $R_{tc}$  was set at location (IV). The symmetry boundary condition is applied at the location of (V) in Fig. 3.

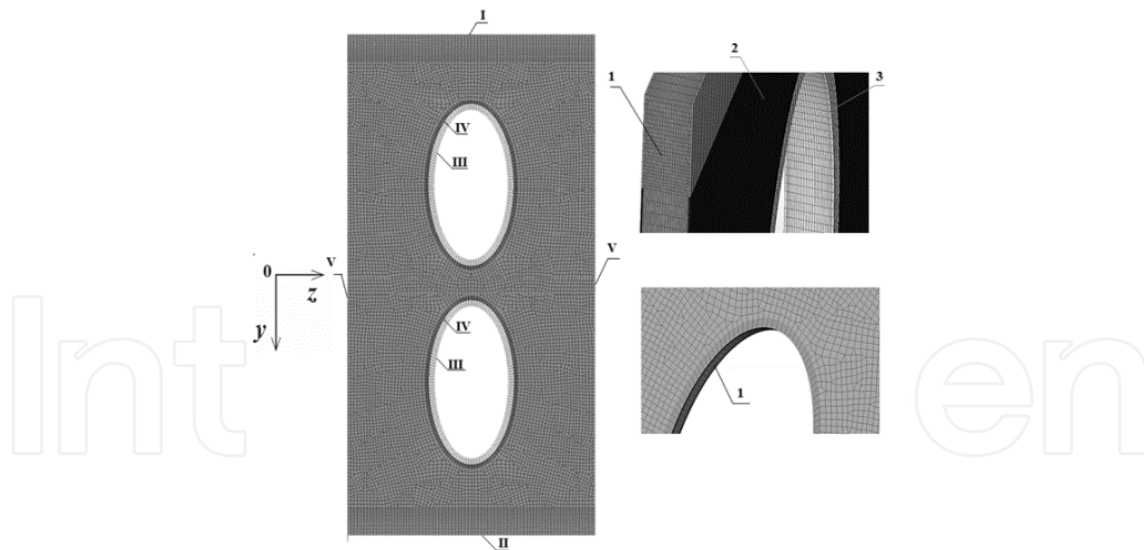


**Figure 3.** Flow passage studied during the computations: 1 –air, 2 – fin, 3 – tube; boundary conditions: I – inlet, II – outlet, III – convective surface, IV – solid \ solid interface (thermal contact resistance), V – symmetry.

The numerical mesh, shown in Fig. 3 was used in the computation (the number of nodes: 452917, the number of elements: 404560). The grid independence tests were performed for the mass averaged outlet air temperature. Refining this numerical model does not lead to the relative change in the obtained results more than 0.1 %. The global imbalance of mass,

momentum and energy equations were less than 0.1%. The boundary flow region computational accuracy was controlled by the so-called  $y^+$  value which was less than 3 in the present computations.

The CFD simulation results, obtained for the following parameters:  $w_0 = 0.8$  m/s,  $T'_a = 14.98$  °C,  $h_w = 1512$  W/(m<sup>2</sup>·K),  $T_w = 73.85$  °C,  $R_{tc} = 0$  (m<sup>2</sup>·K)/W are presented in Fig. 4 [19].

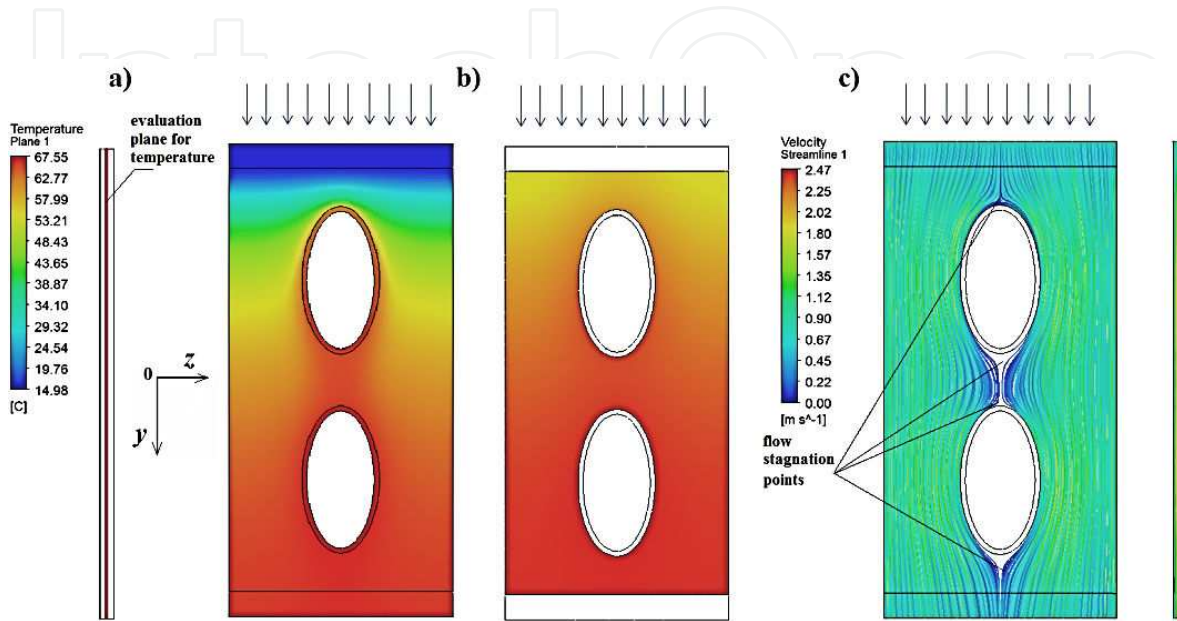


**Figure 4.** The results of test CFD simulation: a) air temperature distribution at the symmetry plane between two neighboring fins b) fin temperature c) air velocity distribution at the symmetry plane between two neighboring fins.

The temperature variations for the air and tube are shown in Fig. 4a. The air temperature is determined at the middle plane between fins. Figure 4b shows fin surface temperature while Figure 4c plots the air velocity distribution. The considerable increase of air temperature can be observed in the first tube row. The increase is larger compared to the second tube row (Fig. 4a). Also, the temperature difference between the fin surface and air is larger in the first row than in the second. Fig 4a and 4b reveals that the temperature difference between the fin surface and fluid is large in the entrance region, what in turn increases the heat flow rate. The efficient heat transfer at the inlet section is the main reason of the significant heat flow rate transferred from water to air in the first row of tubes.

In the existence of the low velocity region between the tubes along the symmetry plane, where the wake behind the upstream tube is bounded by the stagnation on the downstream one (Fig. 4c), the fin temperature (Fig. 4b) in the second tube row is high. Due to the recirculation zones the air entrapped in the vortices is heated almost up to the fin temperature (Fig. 4a). In this region the heat flow rate is close to zero, since the temperature difference between the fin surface and recirculating air is close to zero [19].

The presence of two dead-air zones near the tubes located in the second row decrease the heat flow rate from the second tube row to air. The average heat flux  $q$  at the outer tube surface on the length of one pitch  $s$  between two  $y$  coordinates:  $\bar{y}_n$  and  $\bar{y}_{n+1}$  (Fig. 5) can be calculated as [19]:

$$q(\bar{y}_{n+1/2}) = q\left(\frac{\bar{y}_n + \bar{y}_{n+1}}{2}\right) = \frac{\int_{A_o} q_o dA_o + \int_{A_c} q_c dA_c}{A_o + A_c} \Bigg|_{\bar{y}=\bar{y}_n}^{\bar{y}=\bar{y}_{n+1}} \quad (14)$$

with:

$dA_o$  - the elemental surface area on the outer surface of the oval tube,

$dA_c$  - the elemental surface area on the contact surface between fin and tube,

$q_o$  - the heat flux from the outer tube surface to the air across the elemental surface  $dA_o$ ,

$q_c$  - the heat flux from the outer tube surface to the fin base across the elemental surface  $dA_c$ ,

$\bar{y}$  - the vertical distance from horizontal plane passing through the center of the oval tube to the elevation of the point situated on the tube outer surface.

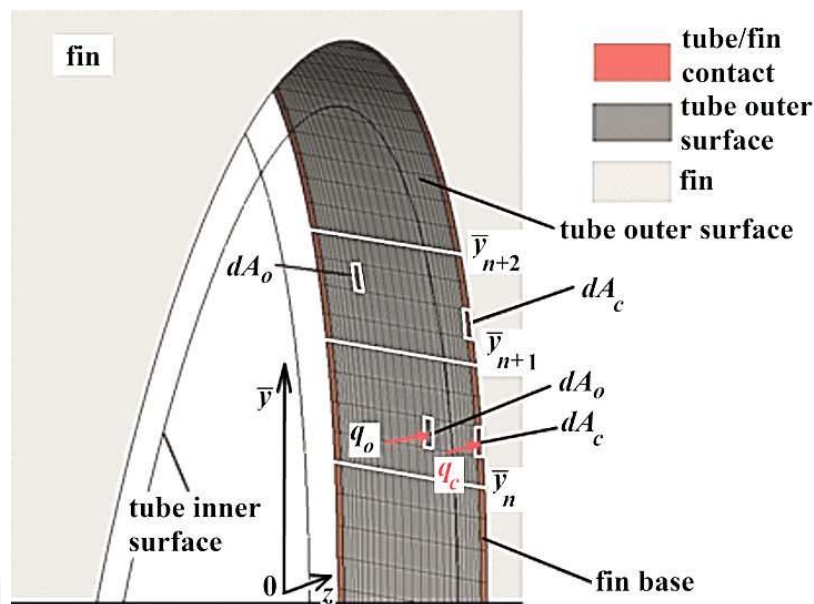


Figure 5. The outer surface of oval tube (grey elements) and the contact surface between fin and tube (red elements).

The variation of outer surface heat flux with the direction of air flow, is presented in form of dimensionless coordinate  $\xi$ ,

$$\xi = -\frac{2\bar{y}}{d_{\max}} \quad (15)$$

The symbol  $\bar{y}$  denotes a distance in the vertical direction between the horizontal plane passing through the oval gravity center '0' and the point located at the outer surface of the tube wall.

Figure 6 [19] shows the variation of the heat flux  $q$  with the dimensionless major radius  $\xi$  of the oval tube for the first and second tube rows.

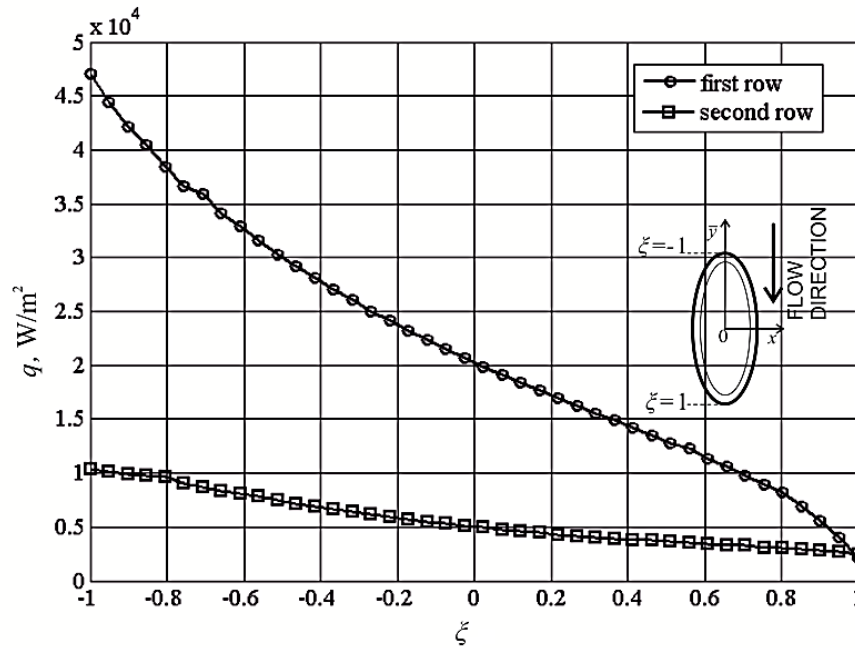


Figure 6. The variations of heat flux  $q$  on the outer surface of tube wall for the first and second row.

The heat flux  $q$  reaches its highest value equal to  $q = 4.72 \cdot 10^4 \text{ W/m}^2$  in the first row at the inflow surface of the oval profile ( $\xi = -1$ ), i.e. front stagnation point. In the area of the rear stagnation point ( $\xi = 1$ ), the considerable heat flux decrease can be observed in both the first and second tube row. In the rear stagnation point on the tube in the first row, the heat flux is only  $q = 2.04 \cdot 10^3 \text{ W/m}^2$ .

The heat transfer is more efficient in the first row of tubes, than in the second. The mean (area-weighted) values of heat flux in the first and second tube row are:  $\bar{q}_I = 2.19 \cdot 10^4 \text{ W/m}^2$  and  $\bar{q}_{II} = 5.62 \cdot 10^3 \text{ W/m}^2$ , respectively. Thus the average value falls almost four times.

In subsections, 4.1 and 4.2 two methods of determining the air-side heat transfer coefficient are presented. The first considers the application of the analytical model of fin-and-tube heat exchanger while the second allows determining the air-side heat transfer coefficient directly from CFD simulations.

#### 4.1. Determination of the gas-side heat transfer coefficient using the analytical model of fin-and-tube heat exchanger and CFD simulation results

The CFD calculations allow to determine the temperature and heat flux distributions in heat transfer domains. It should be noted that the local and average heat transfer coefficients are difficult to determine due to the unclear definition of fluid bulk temperature. From the definition the local heat transfer coefficient is calculated as a ratio of the local heat flux and

difference between the fin surface temperature and air temperature (averaged in the referred flow cross-section). In the case that the average temperature of the air is calculated as the arithmetic mean of the inlet and outlet temperature, the fin surface temperature at the inlet section of a channel formed by the fins is lower than the air mean temperature and then the calculated local heat transfer coefficient can be negative. This is due to a large change in air temperature with the flow direction. Another possibility of determining the average heat transfer coefficient is to calculate first the local distribution of the heat transfer coefficient and then its average value. Nevertheless, this method encounters difficulties in evaluating the local mass-averaged temperature of the air (air bulk temperature) due to the different directions of air flow in the duct between the fins (in vicinity of flow stagnation zones).

A method for determining heat transfer coefficient [18], presented in this study, aims to avoid defining the bulk temperature of air, local or average for the entire flow passage. The method is appropriate for determining the average heat transfer coefficient using the analytical solution for the temperature distribution of air flowing through the two row fin-and-tube heat exchanger. The method is compatible with experimental predictions of heat transfer correlations.

The mean heat transfer coefficient on the air side is determined from the condition that the air temperature increase over two rows of tubes, is the same for the analytical method and for the CFD calculations (Fig. 7a) [19]. To compare the air temperature difference in the heat exchanger, the inlet and outlet air temperatures obtained from the CFD simulations should be mass weighted over the inlet and outlet cross-sections. From the comparison of the difference of the air mass averaged temperatures between the inlet and outlet cross-sections with analytical temperature difference, the average heat transfer coefficient on the air side is computed. The analytical model assumes that the air side heat transfer coefficient is constant. Fig. 7b depicts the positions of evaluation planes used in the CFD simulations to determine the mass-weighted air temperatures.

The average heat transfer coefficient  $h_a$  on the tube and fin surface is determined from the condition that the total mass average air temperature difference  $\Delta\bar{T}_{to,CFD}$  computed using ANSYS CFX program is equal to the air temperature difference  $\Delta T_{to}(R_{tc}, h_a)$  calculated from an analytical model

$$\Delta T_{to}(R_{tc} = 0, h_{a,CFD}) - \Delta\bar{T}_{to,CFD} = 0 \quad (16)$$

The total air temperature difference  $\Delta T_{to}$  is

$$\Delta T_{to} = T_a''' - T_a' = \Delta T_{I} + \Delta T_{II} \quad (17)$$

where  $\Delta T_{I} = T_a'' - T_a'$  and  $\Delta T_{II} = T_a''' - T_a''$  is the air temperature increase over the first and second tube row, respectively (Fig. 7a).

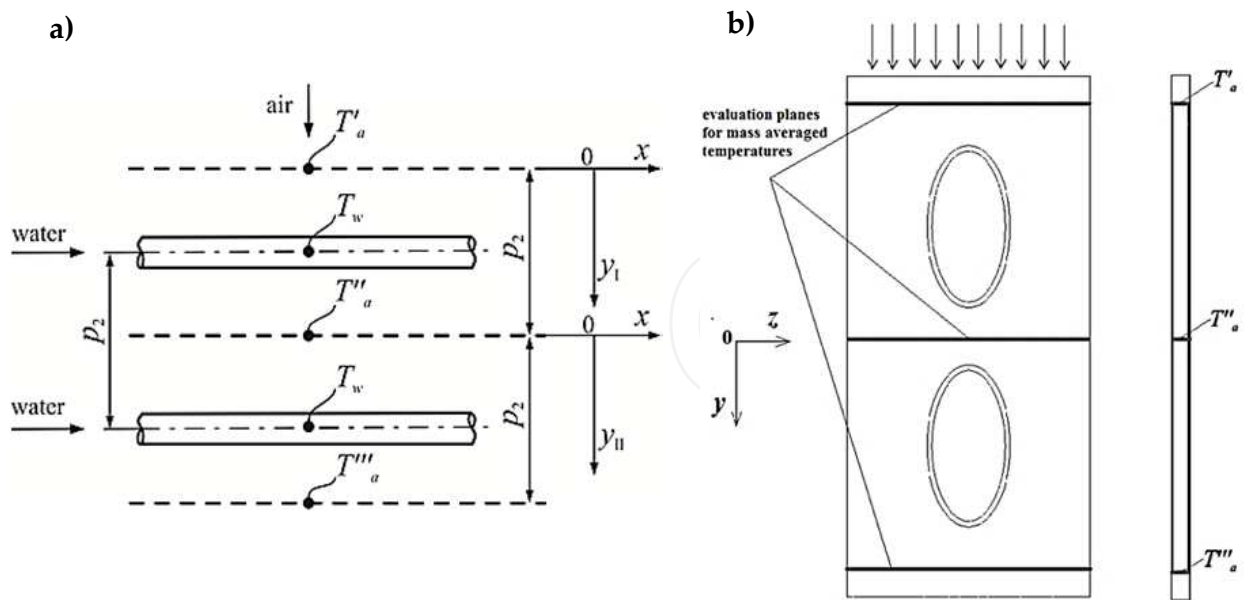


**Figure 7.** Cross flow heat exchanger with two rows of tubes: a) air flow passage used in analytical model, b) evaluation planes for mass averaged temperatures  $T'_a$ ,  $T''_a$  and  $T'''_a$  used in CFD simulations.

The average heat transfer coefficient  $h_a$  over two rows of tubes is calculated by solving equation (16). This study assumes the same water temperature  $T_w$  in the first and the second tube. This small temperature difference has insignificant influence on the average heat transfer coefficient  $h_a$ . Furthermore, the water temperatures are assumed as constant along the tube length. Under these assumptions, the following differential equations with appropriate boundary conditions describe the air temperature [19]

$$\frac{dT_a(y_1^+)}{dy_1^+} = N_a^I [T_w - T_a(y_1^+)] \quad (18)$$

$$T_a \Big|_{y_1^+=0} = T'_a \quad (19)$$

$$\frac{dT_a(y_{II}^+)}{dy_{II}^+} = N_a^{II} [T_w - T_a(y_{II}^+)] \quad (20)$$

$$T_a \Big|_{y_{II}^+=0} = T''_a \quad (21)$$

Solving the initial-boundary problems (18-19) and (20-21) yields

$$T_a(y_I^+) = T_w + (T'_a - T_w) e^{-N_a^I y_I^+} \quad (22)$$

$$T_a(y_{II}^+) = T_w + (T'_a - T_w) e^{-(N_a^I + N_a^{II}) y_{II}^+} \quad (23)$$

where

$$N_a^I = U_o^I A_o / (\dot{m}_a c_{pa}), \quad N_a^{II} = U_o^{II} A_o / (\dot{m}_a c_{pa})$$

The symbols  $\dot{m}_a$  and  $A$  denote the air mass flow rate and the outer surface area of the bare tube, respectively. The overall heat transfer coefficient referred to surface area  $A_o$  can be expressed as [15, 19-22]:

$$U_o = \frac{1}{\frac{A_o}{A_{in}} \frac{1}{h_{in}} + \frac{2A_o}{A_{in} + A_o} \frac{\delta_t}{k_t} + \frac{1}{\bar{h}_a}} \quad (24)$$

with:  $A_{in}$  – area of the inner tube surface,  $\delta_t$  – the thickness of tube wall,  $k_t$  – the thermal conductivity of the tube,  $h_{in}$  – the water side heat transfer coefficient. The equivalent air-side heat transfer coefficient  $\bar{h}_a$  referred to the tube outer surface area  $A_o$  is defined as:

$$\bar{h}_a = \frac{A_f \eta_f(R_{tc}, h_a) + A_e h_a}{A_g} \quad (25)$$

where [19]

$$\eta_f(R_{tc}, h_a) = \frac{(c_1 + c_3 R_{tc} + c_5 h_a + c_7 R_{tc}^2 + c_9 h_a^2 + c_{11} R_{tc} h_a)}{(1 + c_2 R_{tc} + c_4 h_a + c_6 R_{tc}^2 + c_8 h_a^2 + c_{10} R_{tc} h_a)} \quad (26)$$

The unknown coefficients in the function (26) were estimated by the Levenberg – Marquardt method using a commercial software Table Curve 3d version 4.0 [36]. The coefficients appearing in the function  $\eta_f(R_{tc}, h_a)$  are shown in Table 2 [19].

The differences of air temperature over the first and second tube row can be calculated as follows

Coefficient	Value
$c_1$	0.999
$c_2$	3.100
$c_3$	4.850
$c_4$	$2.100 \cdot 10^{-3}$
$c_5$	9.626
$c_6$	-1625.550
$c_7$	-3192.846
$c_8$	-6.763
$c_9$	-2.013
$c_{10}$	221.620
$c_{11}$	$3.260 \cdot 10^{-3}$

**Table 2.** The coefficients of function  $\eta_f(R_{tc}, h_a)$  given by expression (26) [19].

$$\Delta T_I = T_a \Big|_{y_I^+ = 1} - T_a \Big|_{y_I^+ = 0} = (T_w - T'_a) \left( 1 - e^{-N_a^I} \right) \quad (27)$$

$$\Delta T_{II} = T_a \Big|_{y_{II}^+ = 1} - T_a \Big|_{y_{II}^+ = 0} = (T_w - T'_a) e^{-N_a^I} \left( 1 - e^{-N_a^{II}} \right) \quad (28)$$

Assuming that the heat transfer coefficients in the first and second tube row are equal, i.e.  $h_a^I = h_a^{II} = h_a$  and the water side heat transfer coefficient  $h_{in}$  is the same in both tubes results in the equality of the numbers of heat transfer units across the first and second row, i.e.  $N_a = N_a^I = N_a^{II}$ . Hence, the total temperature difference  $\Delta T_{to}$  over two rows can be defined as

$$\Delta T_{to} = \Delta T_I + \Delta T_{II} = (T_w - T'_a) \left( 1 - e^{-2N_a} \right) \quad (29)$$

The temperature difference  $\Delta T_{to}$  given by expression (29) and Eq. (17) are nonlinear functions of the heat transfer coefficient  $h_a$ . Also, the overall heat transfer coefficient  $U_o = U_o^I = U_o^{II}$  is a nonlinear function of  $\bar{h}_a$ , which in turn depends on  $h_a$ . The expression (29) is used in Equation (16) to evaluate the heat transfer coefficient  $h_a$  while the temperature difference  $\Delta \bar{T}_{to,CFD}$  obtained from the CFD simulations is assumed as a measured temperature difference.

## 4.2. Determination of the gas-side heat transfer coefficient directly from CFD simulations of fin-and-tube heat exchanger

The method of determining the average heat transfer coefficient directly from CFD simulation was presented in [20]. The average heat transfer coefficients can be calculated, based on the following relationship:

$$h_{avg,CFD} = \frac{Q}{A_t (\bar{T}_{wall} - T_{\infty})}, \quad (30)$$

where the heat transfer rate, referenced to a single pitch, is:

$$Q = \dot{m} (i_{0,outlet} - i_{0,inlet}), \quad (31)$$

where  $\dot{m}$  denotes the mass flow rate of the air,  $i_{0,outlet}$  and  $i_{0,inlet}$  are the air static enthalpy calculated at the outlet and inlet of the flow passage, respectively. The total heat transfer area is calculated as:

$$A_t = A_f + A_e, \quad (32)$$

the area averaged wall temperature is defined as:

$$\bar{T}_{wall} = \frac{1}{A_t} \int_{A_t} T_{wall} dA, \quad (33)$$

the air bulk temperature  $T_{\infty}$  is calculated as the arithmetic mean temperature from the air inlet and outlet temperatures:

$$T_{\infty} = \bar{T}_a = 0.5 (T_a' + T_a'''). \quad (34)$$

Correlations for air-side heat transfer coefficient will be determined using both methods presented in this chapter. If the air temperature increase  $(T_a''' - T_a')$  is small then both procedures described in the sections 4.1 and 4.2 give the same results.

## 5. Results and discussion

### 5.1. The correlation on gas-side heat transfer coefficient obtained directly from CFD simulations

Table 3 lists the flow and heat transfer parameters studied during the performed computational cases [20]. Moreover the values of the computed outlet air temperature  $T_a'''$  are given in Table 3.

Case	$w_0, m/s$	$T'_a, ^\circ C$	$h_{in}, W/(m^2 K)$	$\bar{T}_w, ^\circ C$	$T''_a, ^\circ C$
1	1				62.59
2	1.2				61.44
3	1.4				60.14
4	1.6				58.71
5	1.8	14.98	4795	65	57.29
6	2				55.86
7	2.2				54.46
8	2.4				53.14
9	2.5				52.51
10	1				29.23
11	1.2				28.87
12	1.4				28.45
13	1.6				28.01
14	1.8	14.98	4795	30	27.56
15	2				27.13
16	2.2				26.70
17	2.4				26.30
18	2.5				26.11

**Table 3.** The list of the computational cases used in the CFD simulations and the values of inlet air velocity  $w_0$ , inlet air temperature  $T'_a$ , the average heat transfer coefficient for water flow  $h_{in}$ , average temperature of water  $\bar{T}_w$  and outlet temperature of the air  $T''_a$

The determined values of the average heat transfer coefficients  $h_{avg.CFD}$  are listed in Table 4 [20]. The computations were carried out for the mean water temperatures:  $\bar{T}_w = 30\text{ }^\circ C$  and  $\bar{T}_w = 65\text{ }^\circ C$ , respectively, to demonstrate that the influence of the tube wall temperature on the determined air side heat transfer coefficients is insignificant. The maximum relative difference between the heat transfer coefficients for  $\bar{T}_w = 30\text{ }^\circ C$  and  $\bar{T}_w = 65\text{ }^\circ C$  does not exceed 2.9 %. These discrepancies are due to different temperature in the boundary layer, which in turn affects the value of thermal conductivity and kinematic viscosity of air, although the air side Prandtl number is 0.7 in both cases. A similar effect of wall temperature on the value of heat transfer coefficient on the air side can be expected in experimental studies [20].

Case no.	$w_0, m/s$	$Q, W$	$\bar{T}_{wall}, ^\circ C$	$\bar{T}_a = T_\infty, ^\circ C$	$h_{avg,CFD}, W/(m^2 K)$
1	1	0.8609	59.049	37.014	39.385
2	1.2	1.0089	58.059	36.521	47.121
3	1.4	1.1445	57.152	36.066	54.155
4	1.6	1.2678	56.321	35.651	60.347
5	1.8	1.3804	55.569	35.275	65.849
6	2	1.4806	54.865	34.922	70.589
7	2.2	1.575	54.247	34.614	74.774
8	2.4	1.6608	53.672	34.326	78.506
9	2.5	1.7007	53.403	34.191	80.204
10	1	0.2570	28.228	21.604	38.913
11	1.2	0.3010	27.938	21.459	46.399
12	1.4	0.3405	27.661	21.321	53.069
13	1.6	0.3765	27.416	21.198	58.935
14	1.8	0.4091	27.186	21.083	64.106
15	2	0.4392	26.989	20.985	68.628
16	2.2	0.4662	26.798	20.889	72.563
17	2.4	0.4913	26.625	20.803	76.083
18	2.5	0.5039	26.551	20.765	77.804

**Table 4.** The values of the heat transfer rate  $Q$  referenced to a single pitch, the area averaged wall temperature  $\bar{T}_{wall}$ , the bulk temperature of the air  $T_\infty$  and the average heat transfer coefficient  $h_{avg,CFD}$  for the air flow, obtained for the computational cases listed in Table 1

The values of  $h_{avg,CFD}$  obtained when  $\bar{T}_w = 30^\circ C$  and  $\bar{T}_w = 65^\circ C$  do not differ significantly for the same air velocity. Table 5 [20] lists the Nusselt number correlation obtained from CFD simulations.

No.	Correlation – CFD simulations	Estimated parameters
1	$Nu_a(T_\infty = 65^\circ C) = x_1 Re_a^{x_2} Pr_a^{1/3}$ $150 < Re_a < 400$ $Pr_a = 0.7$	$x_1 = 0.0674 \pm 0.00621$ $x_2 = 0.7152 \pm 0.0612$
2	$Nu_a(T_\infty = 30^\circ C) = x_1 Re_a^{x_2} Pr_a^{1/3}$ $150 < Re_a < 400$ $Pr_a = 0.7$	$x_1 = 0.0623 \pm 0.00574$ $x_2 = 0.7336 \pm 0.0703$

**Table 5.** Nusselt number formulas for the air flow  $Nu_a$  obtained from the CFD simulations based on the mean arithmetic temperatures of the air:  $T_\infty = 65^\circ C$  and  $T_\infty = 30^\circ C$

The air-flow Nusselt number correlations obtained from CFD simulations are compared with the experimental correlations listed in Table 1. Fig. 8 reveals that the correlations for the air-flow Nusselt number, determined via the CFD simulations, predicts slightly lower values than the one obtained via the measurements. The maximum percentage differences can be observed for  $Re_a = 150$ , where the values of the Nusselt number, obtained using the CFD simulations are from 10.1 % to 13.7% lower than those obtained from the measurements. For the largest value of  $Re_a$  ( $Re_a = 400$ ) these differences are smaller: from 0.5 % to 8.4 % [20].

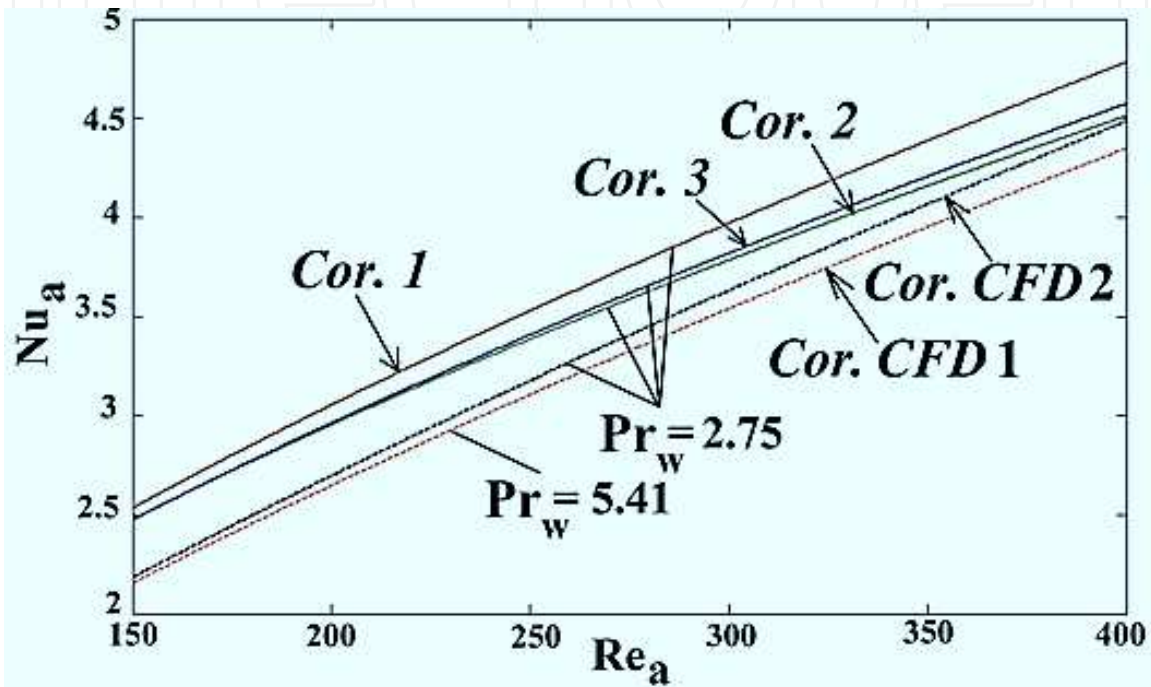


**Figure 8.** The values of the Nusselt number of the air  $Nu_a$  obtained for the Reynolds numbers  $Re_a = 150 - 400$  and the Prandtl number  $Pr_a = 0.7$ , using the correlations listed in Table 1 (experimental correlations: Cor. 1 – Cor. 3) and in Table 5 (correlations based on CFD: Cor. CFD 1, Cor. CFD 2).

The values of the Prandtl numbers for the air and water:  $Pr_a = 0.7$  and  $Pr_w = 2.75$  are typical for air temperatures  $\bar{T}_a$  from 10 °C to 40 °C and for water temperature  $\bar{T}_w = 65$  °C. Fig. 8 and Fig. 9 reveal that the experimental correlation 1 (see Table 1) predicts the largest values of the Nusselt number for the air flow if  $Re_a > 150$  and for water flow if  $Re_w > 10364$ . Experimental correlation 2 predicts the lowest values of the Nusselt number for the air flow if  $Re_a > 150$  and for water flow if  $Re_w > 4000$ . Experimental correlation 3 predicts slightly larger values of  $Nu_a$  if  $Re_a > 150$  and the largest values of  $Nu_w$  if  $Re_w < 10364$ .

During the CFD simulations the idealistic heat transfer conditions were assumed: the constant inlet velocity and the perfect contact between the fin and the outer surface of tube wall. In a real fin-and-tube heat exchanger the maldistribution of air flow as well as the thermal contact resistance between the fin and tube [18, 19] can significantly influence the heat and momentum transfer. Furthermore, the maldistributions of water flow to the tubes of heat exchanger exists for these devices [21-23].The circumstances, mentioned above, explain why the Nusselt

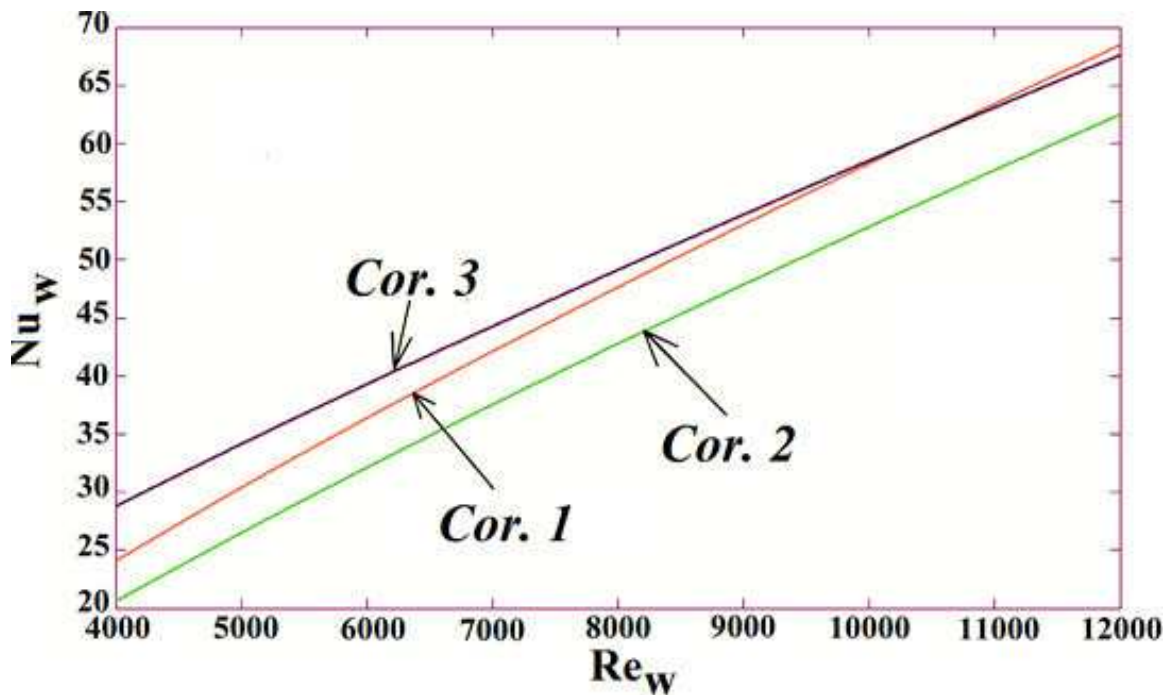


Figure 9. The values of the Nusselt number of water  $Nu_w$  obtained for the Reynolds numbers  $Re_w = 4000 - 12000$  and the Prandtl number  $Pr_w = 2.75$  using the correlations presented in Table 1.

number correlations obtained using CFD simulation differ slightly from the experimental correlations. The analytical-numerical approach for calculating the average thermal contact resistance for a studied fin-and-tube heat exchanger is presented in section 6.

## 5.2. The correlation on gas-side heat transfer coefficient obtained using fin-and-tube heat exchanger model and CFD simulations

Application of the proposed method is illustrated by the following data set[19]:

- air velocity  $w_0$  in front of heat exchanger: 1 m/s – 2.5 m/s,
- air temperature before the heat exchanger  $T'_a = 14.98$  °C,
- mean water temperature in the tubes  $T_w = 68.3$  °C,
- water side heat transfer coefficient  $h_{in} = 4793.95$  W/(m<sup>2</sup>·K).

The temperatures  $T'_a$ ,  $T_w$ , and the heat transfer coefficient  $h_{in}$  were held constant, while the inlet air velocity  $w_0$  was varied from  $w_0 = 1$  m/s to  $w_0 = 2.5$  m/s (Table 6). First, the CFD simulations were performed without including thermal contact resistance ( $R_{tc} = 0$ ). Table 6 [19] lists the air temperature differences obtained from the CFD simulations, for the first and second tube rows ( $\Delta \bar{T}_{I,CFD}$  and  $\Delta \bar{T}_{II,CFD}$ ) as well as the total air temperature difference  $\Delta \bar{T}_{to,CFD}$ . The secant method was employed to solve the nonlinear algebraic equation (16) for the air-side heat transfer coefficient  $h_{a,CFD}$ . The values of  $h_{a,CFD}$  and heat transfer coefficients  $h_{a,me}$  obtained based on the experimental data (correlation 4 in Table 1), are shown in Table 7 [19].

$w_0, m/s$	$\Delta\bar{T}_{I,CFD}, ^\circ C$	$\Delta\bar{T}_{II,CFD}, ^\circ C$	$\Delta\bar{T}_{to,CFD}, ^\circ C$
1.0	41.26	6.37	47.63
1.2	39.03	7.84	46.87
1.4	36.80	9.00	45.80
1.6	34.71	9.84	44.55
1.8	32.79	10.44	43.23
2.0	31.04	10.82	41.86
2.2	29.47	11.05	40.52
2.5	27.39	11.19	38.58

**Table 6.** Temperature differences for the first and second row of tubes ( $\Delta\bar{T}_{I,CFD}$  and  $\Delta\bar{T}_{II,CFD}$ ) and the total temperature difference  $\Delta\bar{T}_{to,CFD}$  obtained using CFD simulations for different air inlet velocities  $w_0$

$w_0, m/s$	$Re_a$	$Pr_a$	$j_a^{CFD}, -$	$h_{a,CFD}, W/(m^2\cdot K)$	$h_{a,me}, W/(m^2\cdot K)$
1.0	149.87	0.694	0.026233	67.54	52.31
1.2	180.01		0.026226	81.02	59.19
1.4	210.29		0.025386	91.49	65.68
1.6	240.70		0.024134	99.39	71.87
1.8	271.22		0.022781	105.53	77.81
2.0	301.86		0.021425	110.26	83.53
2.2	332.60		0.020175	114.20	89.06
2.5	378.86		0.018529	118.94	97.04

**Table 7.** Air-side heat transfer coefficient for entire heat exchanger obtained from CFD simulation:  $h_{a,CFD}$  and experimental correlation  $h_{a,me}$  (correlation 4 in Table 1) for different air inlet velocities  $w_0$ .

The air-side Reynolds and Prandtl numbers ( $Re_a$  and  $Pr_a$ ) were calculated as presented in section 3 for the experimental method. For the determined heat transfer coefficients  $h_{a,CFD}$  the heat transfer correlations are derived as follows. First, the Colburn factor  $j_a$  is approximated using the power law function [20]

$$j_a = x_1 Re_a^{x_2} \quad (35)$$

where the Colburn factor  $j_a$  is defined as [19, 20]

$$j_a = Nu_a / (Re_a Pr_a^{1/3}) \quad (36)$$

Based on the heat transfer coefficients  $h_{a,CFD}$  obtained from the solution of Equation (16), the Colburn factors (Table 7)  $j_{a,i}^{CFD} = \text{Nu}_{a,i}^{CFD} / (\text{Re}_{a,i} \text{Pr}_{a,i}^{1/3})$ ,  $i = 1, \dots, 8$ , were calculated. The symbol  $\text{Nu}_{a,i}^{CFD} = h_{a,CFD} \frac{d_h}{k_a}$  is the Nusselt number for  $i$ th data set CFD. The unknown coefficients  $x_1$  and  $x_2$  in the function (35) were determined using the least squares method. The coefficients  $x_1$  and  $x_2$  were selected to minimize the following sum of squares:

$$S = \sum_{i=1}^{n=8} \left( j_{a,i}^{CFD} - x_1 \text{Re}_{a,i}^{x_2} \right)^2 \quad (37)$$

The symbol  $n$  is the number of data sets shown in Table 7.

The coefficients  $x_1$  and  $x_2$  obtained using the least squares method for the data sets listed in Table 5 are:  $x_1 = 0.188$  and  $x_2 = -0.382$ . To find the optimum values of  $x_1$  and  $x_2$  the Levenberg-Marquardt method was used [35]. The MATLAB R2012 curve fitting toolbox [42] was used for this purpose. Figure 10 [19] depicts the obtained correlation  $j_a^{CFD}(\text{Re}_a)$ , also the prediction bounds set at 95 % confidence level are presented.

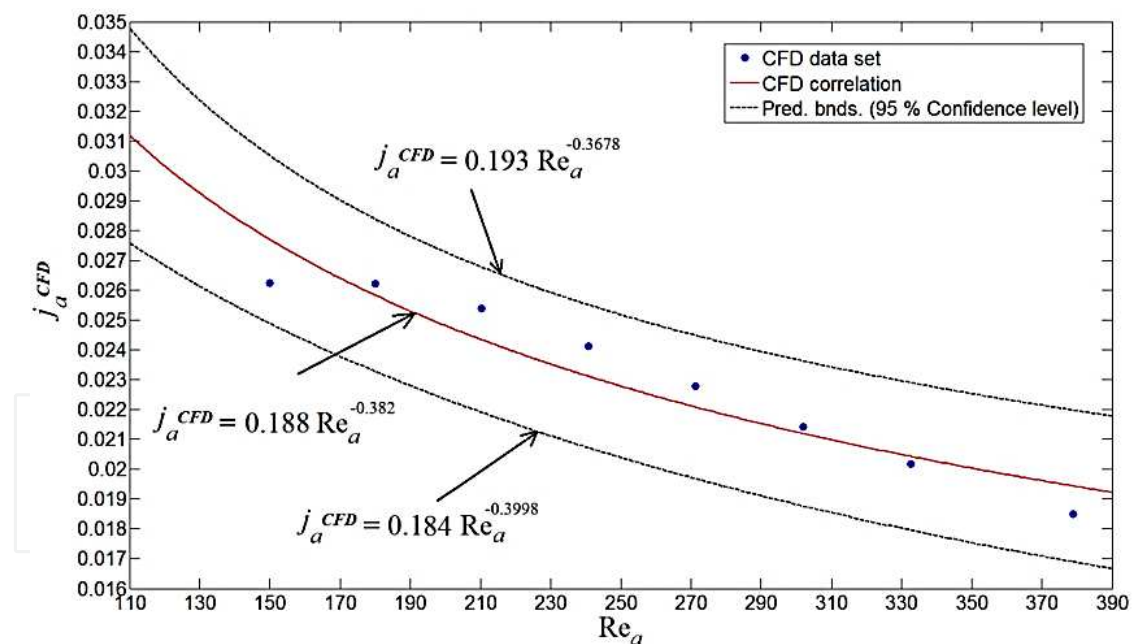


**Figure 10.** Correlation  $j_a^{CFD}(\text{Re}_a) = 0.188 \text{Re}_a^{-0.382}$  - continuous line, and prediction bounds set at 95% confidence level - dashed line. The correlation was based on the CFD data set.

Fig. 10 reveals that the correlation  $j_a(\text{Re}_a) = 0.1878 \text{Re}_a^{-0.382}$  predicts the values of Colburn factor  $j_a^{CFD}$  well for  $\text{Re}_a \in (170, 390)$ . The expression on the air side Nusselt number is obtained after rearranging Eq. (36)

$$\text{Nu}_a = x_1 \text{Re}_a^{(1+x_2)} \text{Pr}_a^{1/3} \quad (38)$$

The following formula for the air-side heat transfer coefficient was obtained after substituting the estimated coefficients  $x_1$  and  $x_2$  into the correlation (38),

$$h_{a,CFD} = \frac{k_a}{d_h} \text{Nu}_a = \frac{k_a}{d_h} 0.188 \text{Re}_a^{0.618} \text{Pr}_a^{1/3} \quad (39)$$

In ref. [37] similar correlations for continuous-fin and tube heat exchangers can be found. The correlation

$$h_a = \frac{k_a}{d_h} 0.174 \text{Re}_a^{0.613} \text{Pr}_a^{1/3} \quad (40)$$

obtained by Kröger [38] is similar to the correlation (39).

The thermal contact resistance exists between the tube and fin for some methods of attaching the fins on the tubes. It reduces the heat transfer rate between the fluids in the heat exchanger.

The correlation (39) leads to over-prediction of the heat transfer rate from the hot to the cold fluid, when the contact resistance occurs. The thermal contact resistance between the tube and the fin base will be determined by using the correlation (39) and the experimental results.

## 6. Estimation of the thermal contact resistance between the tube outer surface and fin base using CFD simulations and experimental data

The correlation for the air-side Nusselt number was derived based on: the experimental data and the CFD simulation. The values of the heat transfer coefficients obtained from the CFD simulation  $h_{a,CFD}$  and from the experiment  $h_{a,me}$  differ from each other (compare Table 1 and Table 7). The method based on the CFD simulation gives larger values of  $h_a$  in comparison to the experimental-numerical method (Table 7). The reason for this discrepancy is the thermal contact resistance between the fin and tube in the tested car radiator.

The air temperature increase across two tube rows  $\Delta \bar{T}_{to,CFD}$  calculated using the heat transfer coefficient  $h_{a,CFD}$  obtained from the CFD based method, is greater than the calculated temperature rise  $\Delta \bar{T}_{to,me}$  obtained with the heat transfer coefficient  $h_{a,me}$ . The temperature differences  $\Delta \bar{T}_{to,CFD}$  and  $\Delta \bar{T}_{to,me}$  can be equal if a thermal contact resistance is included in the CFD simulations.

The air temperature difference  $\Delta \bar{T}_{to,CFD}$  through the entire heat exchanger depends on the thermal contact resistance  $R_{tc}$  and air-side heat transfer coefficient  $h_a$ . To determine the thermal contact resistance  $R_{tc}$ , the nonlinear algebraic equation

$$\Delta \bar{T}_{to,CFD} (R_{tc}, h_{a,CFD}) - \Delta \bar{T}_{to,me} = 0 \quad (41)$$

was solved, for the given values of  $h_{a,CFD}$ , listed in Table 7. The value of the thermal contact resistance  $R_{tc}$  was so adjusted that Eq. (41) is satisfied. Equation (41) was solved using the Secant method. Note that the predicted value of total air temperature difference  $\Delta T_{to,CFD}$  determined from Eq. (29) depends on fin-efficiency  $\eta_f$  which in turns depends on  $R_{tc}$ . Heat transfer coefficient  $h_{a,CFD}$  is a function of air velocity  $w_0$  and is independent of the thermal contact resistance  $R_{tc}$ . The heat transfer coefficient  $h_{a,CFD}$  was calculated using the correlation (39).

Table 8 [19] lists the measurement data sets and the obtained values of thermal contact resistance.

Case	$w_0, m/s$	$T'_{a, ^\circ C}$	$\Delta \bar{T}_{to,me}, ^\circ C$	$T_{w}, ^\circ C$	$\dot{V}_w, dm^3/h$	$h_{in}, W/(m^2 \cdot K)$	$h_{a,CFD}, W/(m^2 \cdot K)$	$R_{tc}, (m^2 \cdot K)/W$
I	1.00	14.98	42.67	68.35	1,892.40	4,793.95	71.14	$4.45 \cdot 10^{-5}$
II	1.27	13.49	39.74	65.02	1,882.20	4,813.42	82.45	$3.27 \cdot 10^{-5}$
III	1.77	13.03	35.83	63.14	1,789.80	4,743.65	101.03	$2.42 \cdot 10^{-5}$
IV	2.20	12.69	31.83	61.24	1,788.00	4,739.78	115.34	$2.42 \cdot 10^{-5}$
							$\bar{R}_{tc}$	$3.16 \cdot 10^{-5}$

**Table 8.** Thermal contact resistance  $R_{tc}$  determined using experimental data sets and the heat transfer coefficient  $h_{a,CFD}$  obtained from the CFD simulations

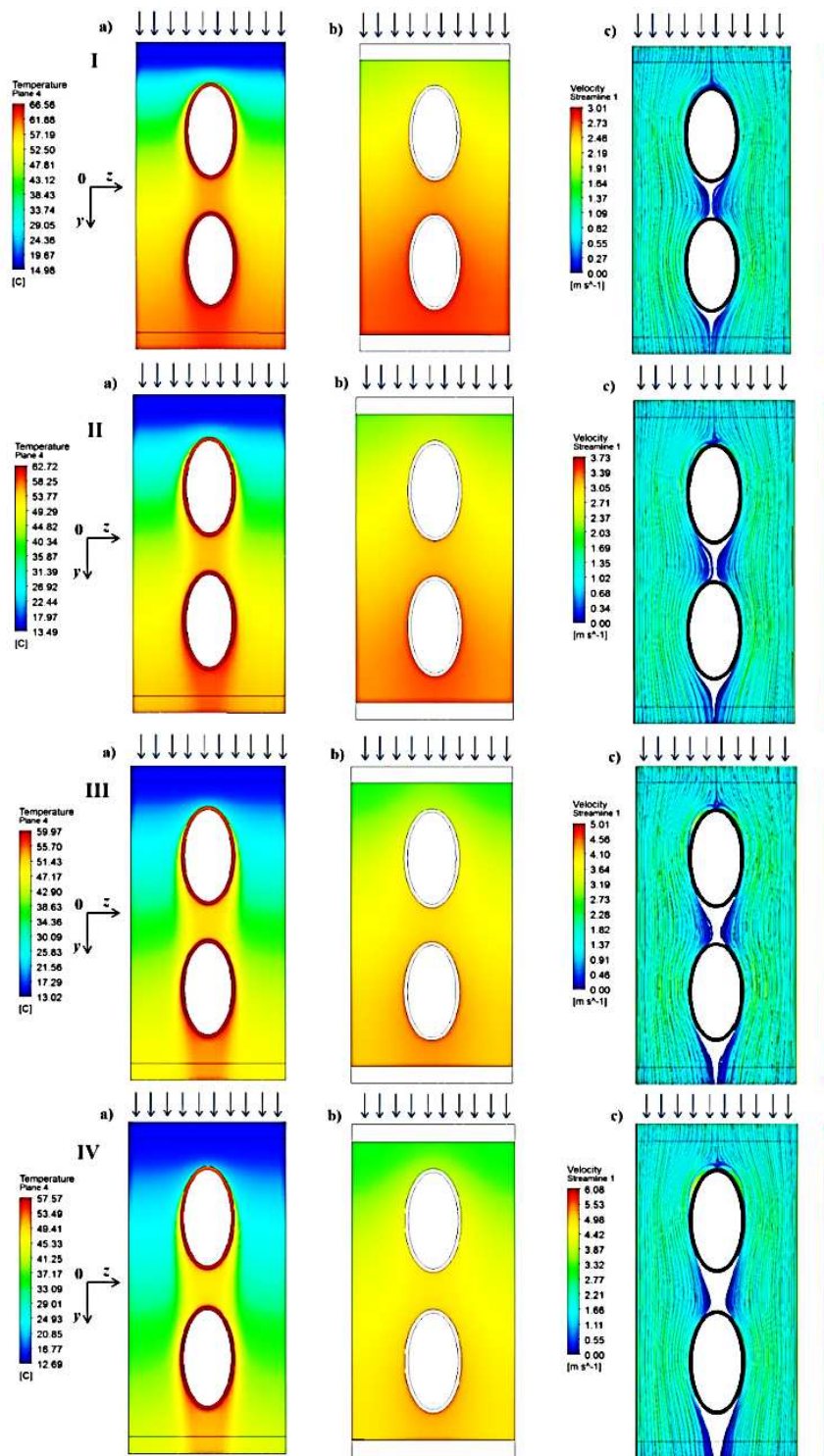
The mean value of thermal contact resistance, obtained for data set given in Table 8, is  $\bar{R}_{tc} = 3.16 \cdot 10^{-5} (m^2 K)/W$ . To calculate the total air temperature differences  $\Delta \bar{T}_{to,CFD}$  the  $\bar{R}_{tc}$  was included in the CFD model of heat exchanger.

Figure 11 presents the results of CFD simulations for computational cases listed in Table 8.

Equation (14) was used to determine the heat flux  $q$  variations at the outer surface of tube wall with dimensionless coordinate  $\xi$ . Fig. 12 presents the results for the first tube row and Fig 13 for the second tube row [19]. Additionally, the computed values of heat flux  $q$  for the thermal contact resistance  $\bar{R}_{tc} = 0 (m^2 K)/W$  are compared with that obtained for  $\bar{R}_{tc} = 3.16 \cdot 10^{-5} (m^2 K)/W$ .

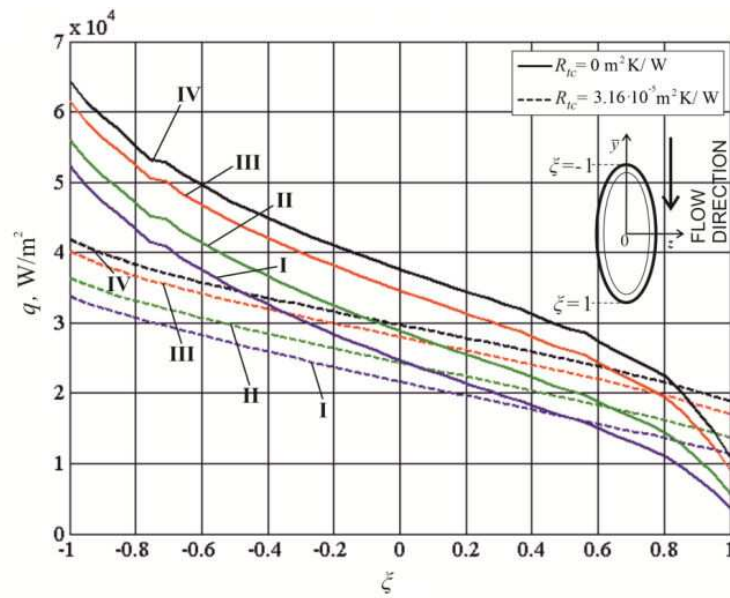
Fig 12 reveals that the thermal contact resistance significantly reduces heat flux through the finned outer surface of the tube. The influence of contact resistance on the average heat flux in the second row of tubes (Fig. 13) is smaller than in the first row of tubes (Fig. 12). The overall heat transfer rate decreases significantly if the thermal contact resistance exists because the largest amount of heat is transferred across the first row of tubes.

Table 9 [19] compares the temperature differences across the two rows of tubes computed using ANSYS CFX for the average thermal contact resistance  $\bar{R}_{tc} = 3.16 \cdot 10^{-5} (m^2 K)/W$  with the



**Figure 11.** The results of CFD simulation for data sets I - IV listed in Table 8: a) temperature distribution in the air domain at the middle of flow passage, b) fin surface temperature, c) air velocity distribution at the middle of flow passage [19].

temperature differences obtained from the expression (29) for the experimentally determined heat transfer coefficient  $h_{a,me}$  (correlation 4, Table 1)



**Figure 12.** The distribution of heat flux  $q$  on the outer surface of tube wall for the first tube row, for computational cases I - IV listed in Table 8.

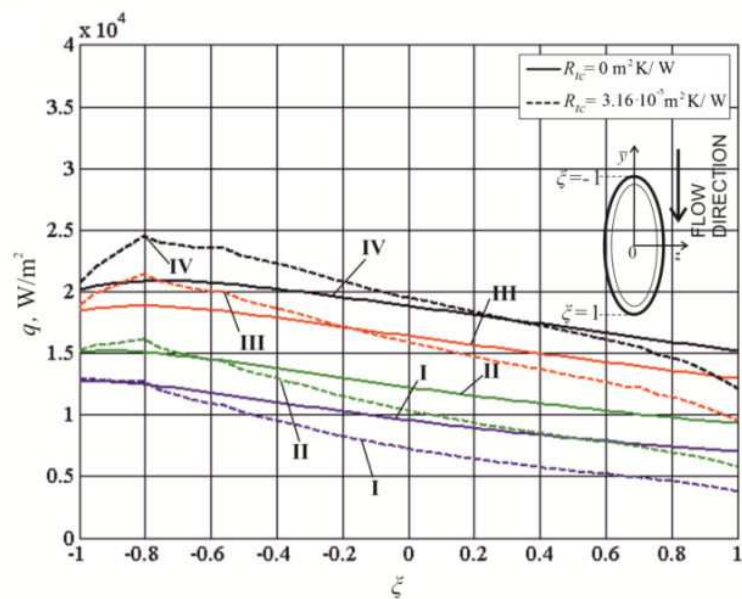


**Figure 13.** The distribution of heat flux  $q$  on the outer surface of tube wall for the second tube row, for computational cases I - IV listed in Table 8.

The relative temperature difference  $|\varepsilon_a|$  between the obtained results, is calculated as:

$$|\varepsilon_a| = \left| \frac{\Delta \bar{T}_t - \Delta \bar{T}_{t,me}}{\Delta \bar{T}_{t,me}} \right| \cdot 100\%. \quad (42)$$

Case	$\Delta \bar{T}_{to,CFD}, ^\circ C$	$\Delta \bar{T}_{to,me}, ^\circ C$	$ \varepsilon_a , \%$
I	44.45	42.67	3.98
II	40.76	39.74	2.52
III	35.46	35.83	1.04
IV	31.16	31.83	2.15

**Table 9.** Air temperature differences  $\Delta \bar{T}_{to,CFD}$  over two rows of tubes obtained using the CFD simulations with the thermal contact resistance  $\bar{R}_{tc} = 3.16 \cdot 10^{-5} \text{ (m}^2 \text{ K)/W}$  and the temperature difference  $\Delta \bar{T}_{to,me}$  obtained from Eq. (29) for the experimentally determined heat transfer coefficients  $h_{a,me}$

The largest value of this difference was obtained for the case I -  $|\varepsilon_a| = 3.98 \%$  (Table 9). For the other computational test cases, the value of  $|\varepsilon_a|$  is less than 3 %. The performed calculations demonstrate the effectiveness of the method developed. The estimated contact resistance can be used in the calculation of equivalent heat transfer coefficient using (Eq. (25)) and in the analytical calculations of the heat transfer rate in the heat exchanger:

$$\dot{Q} = F A_o U_o \Delta T_{lm} \tag{43}$$

where the symbol  $F$  denotes the correction factor based on the logarithmic mean temperature difference  $\Delta T_{lm}$  for a counter-current flow arrangement.

The method proposed for determining the air side heat transfer correlations based on the CFD computations, can easily account for the thermal contact resistance between the tube outer surface and fin bases. The method can also be used for heat exchangers with various tube shapes and other types of the fin to tube attachment as well as for different tube arrangements.

## 7. Conclusions

The experimental and CFD based methods for determining the air-side heat transfer coefficient, for fin-and-tube heat exchanger, are presented in this study. Two types of CFD based methods were described. The first one allows determining the air-side heat transfer coefficient directly from CFD simulations while the second employs the analytical model of fin-and-tube heat exchanger to determine the air-side heat transfer coefficient. The results obtained using these two methods were compared with the experimental data.

Moreover, the method for determination of the thermal contact resistance between the fin and tube was presented. The CFD simulations are appropriate for predicting heat transfer correlations for the plate fin and tube heat exchanger with tubes of various shapes and flow arrangements. Using the experimental data and CFD simulations, the thermal contact resistance between the fin base and tube was estimated. The fin efficiency appearing in the formula for the equivalent air side heat transfer coefficient is a function of the air side heat transfer

coefficient and the thermal contact resistance. The air-side heat transfer correlations are determined based on the CFD simulations. The heat transfer coefficients predicted from the CFD simulations were larger than those obtained experimentally, because in the CFD modeling the thermal contact resistance between the fin and tube was neglected. A new procedure for estimating the thermal contact resistance was developed to improve the accuracy of the heat exchanger calculation. When the value of mean thermal contact resistance, determined by the proposed method, is included in the CFD model, then the computed air temperature distributions show better agreement with measurements.

The computations presented in this study allows to draw the following conclusions. CFD modeling is an effective tool for flow and thermal design of plate fin-and-tube heat exchangers. and is an effective tool for finding heat transfer correlations in the newly designed heat exchangers. However, to obtain good agreement between the CFD modeling and experimental data, it is necessary to adjust some parameters of the CFD model using the experimental results. An example of such a parameter may be thermal contact resistance between the tube and the fin base.

## Nomenclature

$A$ ; area,  $m^2$

$A_{oval}$ ; area of oval cross-section,  $m^2$

$c_p$ ; specific heat at constant pressure,  $J/(kg\ K)$

$c_1 - c_{11}$ ; coefficients of function  $\eta_f(R_{tc}, h_a)$

$d_h$ ; hydraulic diameter of narrow air flow passage,  $m$

$d_{min}, d_{max}$ ; minor/major oval axes,  $m$

$d_i$ ; hydraulic diameter of oval tube,  $m$

$F$ ; correction factor

$h$ ; heat transfer coefficient,  $W/(m^2K)$

$\bar{h}$ ; enhanced heat transfer coefficient based on tube outer surface  $A_o$ ,  $W/(m^2K)$

$j$ ; Colburn j-factor,  $Nu/(Re\ Pr^{1/3})$

$k$ ; thermal conductivity,  $W/(mK)$

$L_i$ ; tube length in car radiator,  $m$

$\dot{m}$ ; mass flow rate,  $kg/s$

$N$ ; number of transfer units

$Nu$ ; Nusselt number

$p_1$ ; pitch of tubes in plane perpendicular to flow,  $m$

$p_z$ ; pitch of tubes in direction of flow, m

$P$ ; perimeter, m

$Pr$ ; Prandtl number

$R_{tc}$ ; mean thermal contact resistance between tube and fin,  $m^2K/W$

$Re$ ; Reynolds number

$q$ ; heat flux,  $W/m^2$

$\bar{q}_I, \bar{q}_{II}$  average heat flux on the outer surface of tube in the first and second tube row,  $W/m^2$

$\dot{Q}$ ; heat flow, W

$s$ ; thickness of air flow passage, m

$T$ ; temperature,  $^{\circ}C$

$\bar{T}_a, \bar{T}_w$  mean temperature of air/water in heat exchanger,  $^{\circ}C$

$U$ ; overall heat transfer coefficient,  $W/(m^2K)$

$\dot{V}$ ; volumetric flow rate,  $dm^3/h$

$w$ ; velocity, m/s;

$w_0$ ; air inlet velocity, m/s;

$w_{max}$ ; maximum air velocity in narrow flow passage, m/s;

$x, y, z$ ; Cartesian coordinates, m

$\bar{y}$  distance, measured along the flow direction, between the oval gravity center and the point located at the outer surface of tube wall, m

$x_i$ ; unknown coefficient

## Greek symbols

$\delta$ ; thickness, m

$\Delta T$ ; air side temperature difference obtained using analytical model of heat exchanger,  $^{\circ}C$

$\Delta \bar{T}$ ; air side temperature difference obtained from the CFD simulations,  $^{\circ}C$

$|\varepsilon_a|$ ; relative change of the air temperature increase, %

$\eta_f$ ; fin efficiency

$\mu$ ; dynamic viscosity,  $Ns/m^2$

$\nu$ ; kinematic viscosity,  $m^2/s$

$\xi$ ; Darcy Weisbach friction factor

## Subscripts

a; air

c; contact area

CFD; obtained using CFD based method

e; external surface of tube between fins

f; fin

g; external surface of tube without fins

in; inner

m; logarithmic mean temperature difference

me; measured temperature difference on air side

min minimum cross-section area for transversal air flow through the tube array

o; outer

t; tube

to; total air side temperature difference

w; water

I, II; first and second tube row, respectively

## Superscripts

'; inlet

''; intermediate

'''; outlet

## Author details

Jan Taler<sup>1\*</sup>, Paweł Ochoń<sup>2</sup>, Dawid Taler<sup>3</sup> and Marzena Nowak-Ochoń<sup>4</sup>

\*Address all correspondence to: [taler@mech.pk.edu.pl](mailto:taler@mech.pk.edu.pl)

1 Cracow University of Technology, Faculty of Mechanical Engineering, Institute of Thermal Power Engineering, Cracow, Poland

2 Cracow University of Technology, Faculty of Mechanical Engineering, Institute of Thermal Power Engineering, Cracow, Poland

3 Cracow University of Technology, Faculty of Environmental Engineering, Institute of Heat Transfer Engineering and Air Protection, Cracow, Poland

4 Cracow University of Technology, Faculty of Mechanical Engineering, Institute of Thermal Power Engineering, Cracow, Poland

## References

- [1] Matos R. S., Vargas J. V. C., Laursen T. A., Bejan A., 2004: Optimally staggered finned circular and elliptic tubes in forced convection, *International Journal of Heat and Mass Transfer* 47(6-7): 1347–1359.
- [2] Jang J. Y., Yang J. Y., 1998: Experimental and Numerical Analysis of the Thermal-Hydraulic Characteristics of Elliptic Finned-Tube Heat Exchangers, *Heat Transfer Engineering* 19(4): 55-67.
- [3] Li. B., Feng B., He Y. L., Tao W.Q., 2006: Experimental study on friction factor and numerical simulation on flow and heat transfer in an alternating elliptical axis tube, *Applied Thermal Engineering*, 26(17–18): 2336–2344.
- [4] Nishiyama H., Ota T., Matsumo T., 1988: Heat Transfer and Flow around an Elliptic Cylinders in Tandem Arrangement, *JSME International Journal Series II*, Vol. 31: 410-419.
- [5] Khan M. G., Fartaj A., Ting D. S. K., 2004: An experimental characterization of cross-flow cooling of air via an in-line elliptical tube array, *International Journal of Heat and Fluid Flow* 25(4): 636–648.
- [6] Saboya F. E. M., Sparrow E. M., 1974: Local and Average Transfer Coefficients for One-Row Plate Fin and Tube Heat Exchanger Configurations, *Journal of Heat Transfer* 96(3): 265-272.
- [7] Saboya S. M., Saboya F. E. M., 1981: Transfer Coefficients for Plate Fin and Elliptical Tube Heat Exchangers, *Proceedings of the VI Brazilian Congress of Mechanical Engineering*, pp. 153-162.
- [8] Bordallo S. N., Saboya F. E. M., 1999: Pressure Drop Coefficients for Elliptic and Circular Sections in One, Two and Three-Row Arrangements of Plate Fin and Tube Heat Exchangers, *Journal of the Brazilian Society of Mechanical Sciences* 21(4): 600-610.
- [9] Idem S., Jacobi A. M., Goldchmidt V. W., 1990: Heat Transfer Characterization of a Finned-Tube Heat Exchanger (with and without Condensation). *Journal of Heat Transfer, Transaction of the ASME*, 112(1): pp. 64-70.

- [10] Hong K. T., Webb R. L., 1996: Calculation of Fin Efficiency for Wet and Dry Fins, *HVAC&R Research* 2(1): 27 -41.
- [11] Taler D., 2002: *Theoretical and experimental analysis of heat exchangers with extended surfaces*, Polish Academy of Science publishing press, ISBN 83-915470-1-9, Poland.
- [12] Zilio C., Cecchinato L., Corradi M., Schiochet G., 2007: An Assessment of Heat Transfer through Fins in a Fin-and-Tube Gas Cooler for Transcritical Carbon Dioxide Cycles, *HVAC&R Research* 13(3): 457-469.
- [13] Taler D., 2004: Determination of heat transfer correlations for plate-fin-and-tube heat exchangers, *Heat and Mass Transfer*, Vol. 40: 809-822.
- [14] Taler D., 2007a: Experimental and numerical predictions of the heat transfer correlations in the cross-flow plate fin and tube heat exchangers, *Archives of Thermodynamics* 28(2): 3-18.
- [15] Taler D., 2007b: Effect of thermal contact resistance on the heat transfer in plate finned tube heat exchangers, ECI Symposium Series, Volume RP5: *Proceedings of 7th International Conference on Heat Exchanger Fouling and Cleaning – Challenges and Opportunities*, pp. 362-371, H Müller-Steinhagen, M. R. Malayeri, P. Watkinson (Eds.), Engineering Conferences International, Tomar, Portugal.
- [16] Taler D., 2009: *Dynamics of Tube Heat Exchangers* (in Polish), Monograph 193, AGH University of Science and Technology Press, ISSN 0867-6631, Cracow, Poland.
- [17] Taler D., 2013: Experimental determination of correlations for average heat transfer coefficients in heat exchangers on both fluid sides, *Heat and Mass Transfer*, Vol. 49. 1125-1139.
- [18] Taler, D., Cebula, A., 2010: A new method for determination of thermal contact resistance of a fin-to-tube attachment in plate fin-and-tube heat exchangers, *Chemical and Process Engineering* 31(4): 839-855.
- [19] Taler D., Ochoń P., Thermal contact resistance in plate fin-and-tube heat exchangers, determined by experimental data and CFD simulations, *International Journal of Thermal Sciences*, Volume 84, October 2014, Pages 309-322.
- [20] Taler D., Ochoń P., Determination of heat transfer formulas for gas flow in fin-and-tube heat exchanger with oval tubes using CFD simulations, *Chemical Engineering and Processing: Process Intensification*, Volume 83, September 2014, Pages 1-11.
- [21] Łopata S, Ochoń P (2010) *Investigation of the flow conditions in a high-performance heat exchanger*, *Arch Thermodyn* 31(3):37–53.
- [22] Łopata S, Ochoń P (2012) *Analysis of operating conditions for high performance heat exchanger with the finned elliptical tube*, *Rynek Energii* 5(102):112–124.

- [23] Łopata S, Ochoń P (2012) Modelling and optimizing operating conditions of heat exchanger with finned elliptical tubes. In: Hector Juarez L (ed) *Fluid dynamics, computational modeling and applications*, InTech, pp 327–356. ISBN:978-953-51-0052-2, Rijeka.
- [24] Ochoń P, Łopata S, Nowak M (2013) Comparative study of conjugate gradient algorithms performance on the example of steady-state axisymmetric heat transfer problem. *Arch Thermodyn* 34(3):15–44.
- [25] Ochoń P, Łopata S, Nowak M, Benim AC (2014) Numerical study on the effect of inner tube fouling on the thermal performance of high-temperature fin-and-tube heat exchanger. *Prog Comput Fluid Dyn* (accepted for print)
- [26] Taler J., Taler D., Sobota T., Cebula A., 2012: Theoretical and Experimental Study of Flow and Heat Transfer in a Tube Bank, in V. M. Pertowa (Ed), *Advances in Engineering Research*, Vol. 1, Nova Science Publishers Inc., pp. 1-56, New York.
- [27] He Y., Tao Y., Tao W., 2008, : Numerical study on the performance of wavy fin heat exchangers with different elliptic tube patterns, *Progress in Computational Fluid Dynamics, An Int. J.* 8 (7/8): 510 – 517.
- [28] Wu Z., Ding G., Wang K., Fukaya M., 2008a: An Extension of a Steady-State Model for Fin-and-Tube Heat Exchangers to Include Those Using Capillary Tubes for Flow Control, *HVAC&R Research*, 14(1): 85-101.
- [29] Liu L., Fan Y., Ling X., Peng H., 2013: Flow and heat transfer characteristics of finned tube with internal and external fins in air cooler for waste heat recovery of gas-fired boiler system, *Chemical Engineering and Processing: Process Intensification*, 74: 142-152.
- [30] Li. B., Feng B., He Y. L., Tao W.Q., 2006: Experimental study on friction factor and numerical simulation on flow and heat transfer in an alternating elliptical axis tube, *Applied Thermal Engineering*, 26(17–18): 2336–2344.
- [31] ANSYS CFX, 2009: Solver Theory Guide r12, ANSYS Inc.
- [32] Chung T. J., 2010: *Computational Fluid Dynamics 2nd ed.*, ISBN 978-0521769693, Cambridge University Press, USA.
- [33] Menter, F. R., 1993: Zonal Two Equation  $k-\omega$  Turbulence Models for Aerodynamic Flows, *AIAA Paper* 93-2906.
- [34] Langtry R. B., Menter F. R., 2005: Transition Modeling for General CFD Applications in Aeronautics, *AIAA paper*.
- [35] Seber G. A. F., Wild C. J., 1989: *Nonlinear Regression*, ISBN 978-0471617600, John Wiley & Sons, New York.
- [36] Table Curve, 2005: *Automated Curve Fitting Software*, AISN Software, Chicago.
- [37] T. Kuppan, *Heat exchanger design handbook*, 2nd ed., CRC Press – Taylor and Francis Group, 2013, Boca Raton.

- [38] D. G. Kröger, *Radiator characterization and optimization*, SAE Paper 840380, 1985, pp. 2.984 – 2.990.
- [39] Gnielinski, V., 1976: Neue Gleichungen für den Wärme- und den Stoffübergang in turbulent durchströmten Rohren und Kanälen, *Forschung im Ingenieurwesen* 41(1): 8-16.
- [40] Pietukhov B. S., Popov V. N., 1963: *Theoretical Calculations of Heat Transfer in Turbulent Flow in Tubes of an Incompressible Fluid with Variable Physical Properties*, High Temperature Institute Paper, 1(1), pp. 69-83 (in Russian).
- [41] Bejan A., 2003: Forced Convection: Internal Flows, Chapter 5 in *Heat Transfer Handbook*, Bejan A. Kraus S. (Eds.), ISBN 978-0-471-39015-2, Wiley, Hoboken.
- [42] MATLAB, 2013: MATLAB online documentation: <http://www.mathworks.com/help/matlab>, MathWorks